Multidimensional Conduction-Band Engineering for Maximizing the Continuous-Wave (CW) Wallplug Efficiencies of Mid-Infrared Quantum Cascade Lasers

Dan Botez, *Fellow, IEEE*, Jae Cheol Shin, Jeremy Daniel Kirch, *Member, IEEE*, Chun-Chieh Chang, Luke James Mawst, *Fellow, IEEE*, and Thomas Earles

(Invited Paper)

***Abstract*—By tailoring the active-region quantum wells and barriers of 4.5–5.0-μm-emitting quantum cascade lasers (QCLs), the device performances dramatically improve. Deep-well QCLs significantly suppress carrier leakage, as evidenced by high values for the threshold-current characteristic temperature T_0 (253 K) and the slope-efficiency characteristic temperature T_1 (285 K), but, due to stronger quantum confinement, the global upper-laser-level lifetime τ_{4g} decreases, resulting in basically the same room-temperature (RT) threshold-current density $J_{\rm th}$ as conventional QCLs. Tapered active-region (TA) QCLs, devices for which the active-region barrier heights increase in energy from the injection to the exit barriers, lead to recovery of the τ_{4g} value while further suppressing carrier leakage. As a result, experimental RT $J_{\rm th}$ values from moderate-taper TA 4.8-μm emitting QCLs are ∼14% less than for conventional QCLs and T_1 reaches values as high as 797 K. A step-taper TA (STA) QCL design provides both complete carrier-leakage suppression and an increase in the τ_{4g} value, due to Stark-effect reduction and strong asymmetry. Then, the RT $J_{\rm th}$ value decreases by at least 25% compared to conventional QCLs of same geometry. In turn, single-facet, RT pulsed and continuous-wave maximum wallplug-efficiency values of 29% and 27% are projected for 4.6–4.8-μm-emitting QCLs.**

***Index Terms*—Lasers, quantum-well lasers, quantum wells (QWs), semiconductor lasers, Stark effect.**

I. Introduction

THE core region of conventional quantum-cascade-laser (QCL) structures [1] is composed of a superlattice of quantum wells (QWs) and barriers of *fixed* alloy composition, respectively. This restriction, rooted in the fact that historically QCLs have been grown by molecular-beam epitaxy (MBE), causes short-wavelength (4.5–5.0 μm) devices to have relatively small energy differences between the upper laser level and the top of the exit barrier [2]: 150–250 meV, which, at room temperature (RT), lead to relatively high electronic temperatures in the upper laser level [3]. In turn, conventional high-performance QCLs emitting in the 4.5–5.0-μm range suffer from severe carrier leakage, which manifests itself as low characteristic-temperature T_0 values (130–150 K) [4]–[7] for the threshold-current density $J_{\rm th}$, and low characteristic-temperature T_1 values (140–170 K) [4], [6], [7] for the slope efficiency $\eta_{\rm sl}$ over wide heatsink-temperature ranges above RT. Since the core-region temperature rise with respect to the heatsink temperature $\Delta T_{\rm act}$ is a strong function of T_0 and T_1 [2], the device heating in CW operation is severe which, in turn, limits conventional-QCL maximum wallplug efficiency $\eta_{\rm wp,max}$ at RT to values of ≤13% [8], [9], for single-facet emitted light, and is the main reason why statistically relevant lifetest data exist *only* for low (<0.2 W) CW powers [7].

The flexibility of the metal-organic chemical vapor deposition (MOCVD) *and* gas-source MBE crystal-growth techniques allows one to vary at will QW and barrier compositions in the QCL active regions (ARs). This permits advanced AR-design optimization by using multidimensional conduction-band engineering, in that the layer thicknesses and compositions are varied independently. We have applied this concept by introducing [10] and demonstrating the deep-well (DW) design concept via which carrier leakage is suppressed, as evidenced by significantly increased T_0 and T_1 values: 253 and 285 K, respectively [4], and the tapered-active (TA) design concept for DW devices [11], [12], [42] which further suppresses carrier leakage and thus led [13] to T_1 values as high as 797 K. Bai *et al*. [14] have obtained T_0 and T_1 values of 244 and 348 K, respectively, for 4.9-μm-emitting QCLs of moderately high injector doping by using the so-called shallow-well design, which is in effect a TA-type QCL design without deep wells [12], [13]. As a result, they achieved a record-high, single-facet, RT CW wallplug efficiency: 21%, still short of predicted limits [15], [16] (i.e., ≈31%). Here, we review and analyze DW- and TA-type QCL-device behavior, and present and analyze an optimized TA-QCL design that leads to both complete carrier-leakage suppression and an increase in upper-level lifetime. Then, projected $\Delta T_{\rm act}$

Manuscript received November 3, 2012; revised December 5, 2012; accepted December 27, 2012. Date of publication January 1, 2013; date of current version May 13, 2013. This work was supported in part by the National Science Foundation under Grant ECCS-0925104.

D. Botez, J. D. Kirch, C.-C. Chang, and L. J. Mawst are with the University of Wisconsin-Madison, Madison, WI 53706 USA (e-mail: botez@engr.wisc.edu; jdkirch@wisc.edu; chang48@wisc.edu; mawst@engr.wisc.edu).

J. C. Shin is with the Photonic-Energy Center, Korea Photonics Technology Institute, Gwangju 500–779, Korea (e-mail: jchshin@gmail.com).

T. Earles is with Intraband, LLC, Madison, WI 53726 USA (e-mail: tearles@tds.net).

Color versions of one or more of the figures in this paper are available online at http://ieeexplore.ieee.org.

Digital Object Identifier 10.1109/JSTQE.2012.2237387

1077-260X/$31.00 © 2013 IEEE

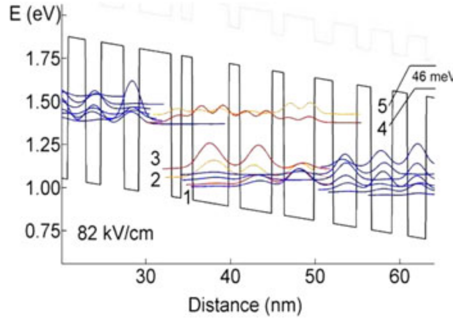

Fig. 1. Conduction band diagram and key wavefunctions for conventional QCL emitting at λ = 4.7 μm. The upper laser level is labeled as 4, while 5 is the next higher energy state in the AR. 3, 2, and 1 are lower energy states in the AR.

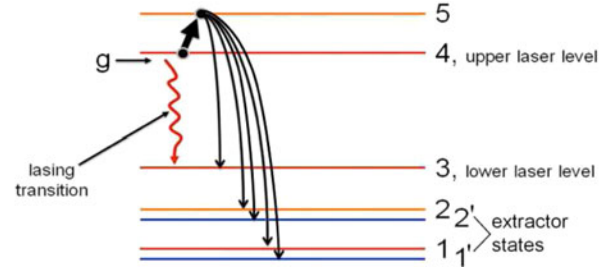

Fig. 2. Schematic representation of the primary leakage paths for electrons injected into the upper laser level of a 4.5- to 5.0-μm emitting QCL of DPR design and $E_{54} \geq 50$ meV. Here, g is the injector-region ground state, 1 through 5 are energy states in the AR, and $1'$ and $2'$ are extractor states penetrating the AR.

values at high drive levels above threshold are significantly smaller than those for published QCLs, thus allowing for QCLs to be able to reach RT CW $\eta_{\rm wp,max}$ values close to theoretically predicted limits.

II. Carrier Leakage and CW Wallplug Efficiency

A. Threshold-Current Density

The threshold-current density $J_{\rm th}$ can be written as follows:

$$J_{\rm th} = \frac{q_0 C}{\tau_{{\rm up},g}} + J_{\rm leak,th} \tag{1}$$

where C is the sum of the ratio of total (optical) losses to modal-gain cross section, and the backfilling factor [4]; $\tau_{{\rm up},g}$ is the global "effective" upper-level lifetime; and $J_{\rm leak,th}$ is the carrier-leakage current density at threshold [4]. For a QCL structure with a double-phonon-resonance (DPR) lower-level depopulation scheme, as that shown for a conventional QCL in Fig. 1, $\tau_{{\rm up},g} = \tau_{\rm 4g}(1-\tau_{\rm 3g}/\tau_{43})$, where $\tau_{\rm 4g}$ and $\tau_{\rm 3g}$ are the global lifetimes in the upper and lower levels, respectively, corresponding to transitions to both lower AR states (e.g., to states 3, 2, 1 from state 4) and to extractor states penetrating into the AR (e.g., the three blue-colored extractor states penetrating the AR in Fig. 1). That is, the global upper-level lifetime can be expressed as

$$\frac{1}{\tau_{\rm 4g}} = \frac{1}{\tau_4}\bigg|_{\rm lower_AR_states} + \frac{1}{\tau_4}\bigg|_{\rm extractor_states_penetrating_AR}. \tag{2}$$

As for the leakage current, we have shown in [4] that for an energy difference between the upper level and the next higher AR energy state, E_{54}, $\geq$50 meV the primary leakage path is *shunt* leakage current through state 5. That is, as shown in Fig. 2, part of the electrons injected into the upper level are thermally excited to state 5 from where most relax to the lower AR states and to extractor states penetrating the AR. Then, $J_{\rm leak,th}$ is proportional to the scattering rate from state 4 to state 5 which is well approximated by [12], [17]

$$\frac{1}{\tau_{45}} \approx \frac{1}{\tau_{54}} \exp\left(-\frac{E_{54}}{kT_{\rm e4}}\right) \tag{3}$$

where $T_{\rm e4}$ is the electronic temperature in state 4 and τ_{54} is the relaxation time from state 5 to state 4. Therefore, in order to effectively suppress carrier leakage, the E_{54} and τ_{54} values should be increased as much as possible while making sure that electrons are kept "cool" in state 4 (e.g., reduce the $T_{\rm e4}$ value by using structures of strong quantum confinement [3] such as deep wells in the AR [4]). Here, it should be emphasized that experimental T_0 values have been accurately predicted for both conventional [4], [5] and deep-well [4] mid-infrared (IR) QCLs *only* by considering hot electrons in the upper level. Furthermore, the fact that the electrons are *hot* strongly affects not only the carrier leakage, but the backfilling current as well [4], [12] since the electronic temperature of the injector ground state is basically the same as $T_{\rm e4}$ [4]. Therefore, the temperature dependence of $J_{\rm th}$ (i.e., the T_0 value) is primarily determined not just by the carrier-leakage current, but by the backfilling current as well, since both are strong functions of temperature.

B. External Differential Quantum Efficiency

The external differential quantum efficiency η_d can be written

$$\eta_d = \eta_p \eta_{\rm tr} \frac{\alpha_m}{\alpha_{\rm tot}} N_p = \left(1 - \frac{J_{\rm leak,th}}{J_{\rm th}}\right) \eta_{\rm tr} \frac{\alpha_m}{\alpha_m + \alpha_w} N_p \tag{4}$$

where η_p, as derived in [12], is the differential pumping efficiency at and close to threshold [4], [12]; $\eta_{\rm tr}$ is the laser-transition differential efficiency [15]; α_m and α_w are the mirror and waveguide losses, respectively; and N_p is the number of periods. The product $\eta_p \eta_{\rm tr}$ can be thought of as the internal *differential* efficiency per period η_i [2], which should not be confused with either the tunneling-injection efficiency into the upper level $\eta_{\rm inj}$ [1], taken here to be unity, or with the internal quantum efficiency. Quite similar to interband-transition devices [18], the factor multiplying the ratio of mirror losses to total losses in the η_d expression is a differential quantity.

The temperature dependence of η_d, as defined by the T_1 parameter [i.e., $\eta_d(T_{\rm ref} + \Delta T) = \eta_d(T_{\rm ref})\exp(-\Delta T/T_1)$, where $T_{\rm ref} + \Delta T$ is the heatsink temperature T_h, and $T_{\rm ref}$ is the reference heatsink temperature], is primarily determined by the variations with temperature of both η_p and α_w [4]. It is worth noting that, just as in the case of interband-transition lasers [19], carrier leakage strongly affects the T_1 value. Thus, T_1 is a much better indicator of carrier leakage than the T_o value since T_o reflects the temperature dependence of the backfilling current as well.

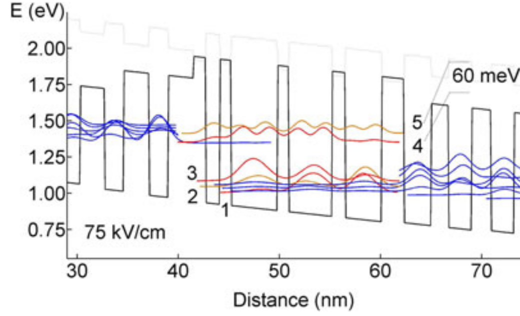

Fig. 3. Conduction band diagram and key wavefunctions for a deep-well QCL emitting at λ = 4.8 μm [24]. The energy states 1 through 5 are defined just as in Fig. 1.

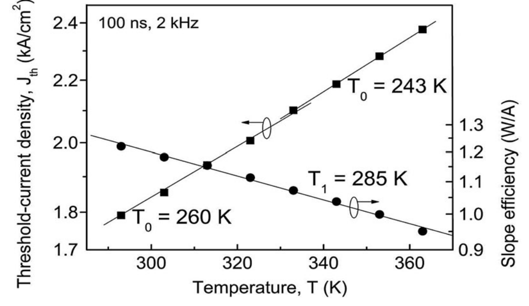

Fig. 4. Deep-well QCLs [24]: $J_{\rm th}$ and the slope efficiency $\eta_{\rm sl}$ as a function of heatsink temperature. T_0 and T_1 are characteristic temperatures for $J_{\rm th}$ and $\eta_{\rm sl}$.

C. Maximum Wallplug Efficiency

The expression for the (pulsed) maximum wallplug efficiency $\eta_{\rm wp,max}$ can be written as [4]

$$\eta_{\rm wp,max} = \eta_s \eta_p \eta_{\rm tr} \frac{\alpha_{m,\rm opt}}{\alpha_{m,\rm opt} + \alpha_w} \left(1 - \frac{J_{\rm th}}{J_{\rm wp,max}}\right) \frac{N_p h\nu}{q_0 V_{\rm wp,max}} \quad (5)$$

where η_s is the droop in the pulsed *L–I* curve at the $\eta_{\rm wp,max}$ point [4], $\alpha_{m,\rm opt}$ is the optimal mirror loss [20], $J_{\rm wp,max}$ is the current density at the $\eta_{\rm wp,max}$ point, $h\nu$ is the photon energy and $V_{\rm wp,max}$ is the voltage at $J_{\rm wp,max}$. The value for $\alpha_{m,\rm opt}$ has been found both theoretically [20] and experimentally [14], [20] to be ∼2.2 cm^{-1}. Analysis of published data reveals that the $J_{\rm wp,max}$ value, in both pulsed and CW operation, is an approximate fixed multiple of the pulsed $J_{\rm th}$ value at RT, $J_{\rm th}$(300 K), that is, $J_{\rm wp,max} \cong$ B$J_{\rm th}$(300 K). For instance, for devices with strong carrier leakage, we found [4] the B value to be ∼2.5. As pointed out below in Section V, for devices with suppressed carrier leakage the B value increases to ∼3.0. As for η_s, its value was found [4] to be ∼0.83 for devices with strong carrier leakage. Just like for $J_{\rm wp,max}$, the η_s value increases for devices with suppressed carrier leakage, such that it reaches ∼0.90 (see Section V). Then, the maximum CW wallplug efficiency, at a heatsink temperature of 300 K, can be expressed as

$$\eta_{\rm wp,max}|_{\rm CW} \approx \eta_s \eta_p \eta_d \exp\left(-\frac{\Delta T_{\rm act}}{T_1}\right) \times \left[1 - \frac{1}{B}\exp\left(\frac{\Delta T_{\rm act}}{T_0}\right)\right] \frac{N_p h\nu}{q_0 V_{\rm wp,max}} \quad (6)$$

where $\Delta T_{\rm act}$ at the $\eta_{\rm wp,max}$ point is given by [2]

$$\Delta T_{\rm act}|_{\eta_{\rm wp,max}} = T_l - T_h = R_{\rm th} P_{\rm el}(1 - \eta_{\rm wp,max}) \quad (7)$$

where T_l is the lattice temperature, $R_{\rm th}$ is the thermal resistance, and $P_{\rm el}$ is the electrical power dissipated in CW operation at the $\eta_{\rm wp,max}$ point (i.e., $P_{\rm el}$ = A $J_{\rm wp,max} V_{\rm wp,max}$, where A is the pumped area). As clearly evident from (6) and (7), both $\eta_{\rm wp,max}$ and $\Delta T_{\rm act}$ are strong functions of the T_o, T_1, and $R_{\rm th}$ values. Therefore, in order to maximize $\eta_{\rm wp,max}$ and to minimize $\Delta T_{\rm act}$ (at the $\eta_{\rm wp,max}$ point), carrier leakage needs to be suppressed (in order to obtain high T_o and T_1 values) and the $R_{\rm th}$ value needs to be reduced as much as possible. From published data on episide-down mounted, buried-heterostructure 4.6–4.8-μm-emitting, conventional QCLs [6], [21], [22], when considering a fixed cavity length (e.g., 5 mm), we find that over the 6–10-μm range in buried-ridge width, w, $R_{\rm th} \propto w^{1.4}$, that is, the thermal conductance, $G_{\rm th} \propto 1/w^{2.4}$. This is expected since a significant portion of heat removal occurs laterally, away from the buried core region. Therefore, w needs to be lowered. However, too narrow a ridge increases the series resistance and decreases output power. A good compromise for the w value appears to be 8 μm, as recently used in devices of the highest CW $\eta_{\rm wp,max}$ reported to date [14].

Other factors that affect the CW $\eta_{\rm wp,max}$ value are $J_{\rm th}$(300 K) and $V_{\rm wp,max}$. That is, for a given injector-region sheet doping density n_s that ensures high-power operation [e.g., n_s in the (0.7–1.0) × 10^{11} cm^{-2} range] and same mirror loss, a decrease in the $J_{\rm th}$(300 K) value reduces both $\Delta T_{\rm act}$ *and* the electronic temperatures in the injector ground state [3] and the upper laser level [3]–[5] which, in turn, lead to increases in both T_o and T_1 values [4], [13]. As will be shown below, for optimized TA–QCL structures, the $J_{\rm th}$(300 K) value can be significantly decreased by both suppressing carrier leakage and increasing the $\tau_{{\rm up},g}$ value. As for $V_{\rm wp,max}$, its value could be reduced without significantly impacting the T_o value by using the "pocket injector" concept [23], that is, carrier injection into the upper laser level from the first injector-region excited state by taking advantage of the fact that that state is strongly populated [23] when electrons in the injector miniband are hot. For the purpose of this study, however, we consider only structures with injection from the injector ground state.

III. Deep Well Versus Conventional QCLs

DW QCLs are devices for which the QWs in the active region of each period are lower in energy than the QWs in the injector regions [10]. The band diagram and relevant wavefunctions for a typical DW–QCL structure [4] are shown in Fig. 3. Details of the structure are given in [24]. The deep wells and associated tall barriers, in the AR, bring about a significant increase in the E_{54} value: from 46 meV, typical of conventional QCLs, to 60 meV [2]. As a result, carrier leakage was substantially suppressed that led to high T_o and T_1 values over the 20–60 °C range in heatsink temperature: 253 and 285 K, respectively (see Fig. 4). However, the value for $J_{\rm th}$(300 K) stayed basically the same. Below, we explain why that happened.

TABLE I
DEEP WELL VERSUS CONVENTIONAL QCL

Parameter	DW QCL	Conventional QCL
τ_4	1.32 ps	1.65 ps
τ_{4g}	1.18 ps	1.305 ps
τ_{3g}	0.24 ps	0.19 ps
$\tau_{up,g}$	1.10 ps	1.23 ps
J_{leak} / J_{th} at 300 K	~ 8.5 %	~15 %

The lifetimes for QCL devices are calculated with the same eight-band k•p code previously used in [4]. As seen from Fig. 1, for conventional QCLs the state-1 wavefunction peaks away from the state-4 wavefunction, such that the τ_{41} lifetime is about twice as large as each of the τ_{42} and τ_{43} lifetimes. More specifically, for the conventional QCL that we analyzed [4], [22] the values for τ_{41}, τ_{42}, and τ_{43}, at a field strength of 82 kV/cm, are 9.08, 4.33, and 3.77 ps, respectively. Thus, the corresponding τ_4 value is relatively large: 1.65 ps. In contrast, for DW QCLs the strong quantum confinement brought about by using deep wells and tall barriers causes the state-1 wavefunction to be pulled towards the injection barrier and thus overlap well with the state-4 wavefunction, such that τ_{41} decreases and becomes comparable to τ_{42} and τ_{43}. For instance, the τ_{41}, τ_{42}, and τ_{43} values calculated for the structure in Fig. 3 are 4.01, 5.15, and 3.2 ps, respectively. The corresponding τ_4 value is 1.32 ps, that is, smaller than in conventional QCLs (see Table I).

Returning to the conventional QCL, due to deep penetration of extractor states into the AR, the τ_{4g} value, calculated as shown in (2), is 1.305 ps, that is, 21% lower than when considering relaxation to only lower AR states 3, 2, and 1. For DW devices, the extractor-states penetration into the AR is less, such that τ_{4g} is 1.18 ps, only 11% less than the τ_4 value. Then, we proceed to calculate the $\tau_{up,g}$ values (see Table I) and see that the net effect is that the $\tau_{up,g}$ value is ~10% lower for DW QCLs compared to conventional QCLs.

However, for DW devices carrier leakage is substantially reduced, such that the RT relative leakage-current density value $J_{leak,th}/J_{th}$ decreases from ~15% to ~8.5% [4]. In turn, the effect of lower $\tau_{up,g}$ value is offset by the lower $J_{leak,th}/J_{th}$ value and one ends up with basically the same J_{th}(300 K) value for both conventional and DW QCLs [4].

IV. Tapered Active-Region QCLs

A. Basic Concept

The basic idea is to increase the barrier heights in the AR from the injection barrier to the exit barrier (e.g., a linear-tapered device, as shown in Fig. 5), the so-called tapered active-region (TA) design [11], [12], [42]. As seen in Fig. 5, by using a linear-taper TA DW design, the E_{54} value can be increased to 84 meV for reasons that will become evident from the study below. The design is different from the DW design in that the Al concentration x of the AR $Al_xIn_{1-x}As$ barriers increases linearly from 0.60 to 0.75, from the injection into the exit barriers, while for DW devices, it is constant throughout the AR at 0.75. Below we perform analyses on pairs of QWs, to give us some intuition as to what happens in the active region of actual TA-type devices.

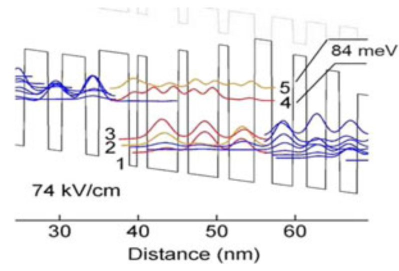

Fig. 5. Conduction band diagram and key wavefunctions for linear-taper TA QCL structure emitting at $\lambda = 4.7$ μm [11], [12], [42]. The energy states 1 through 5 are defined just as in Fig. 1.

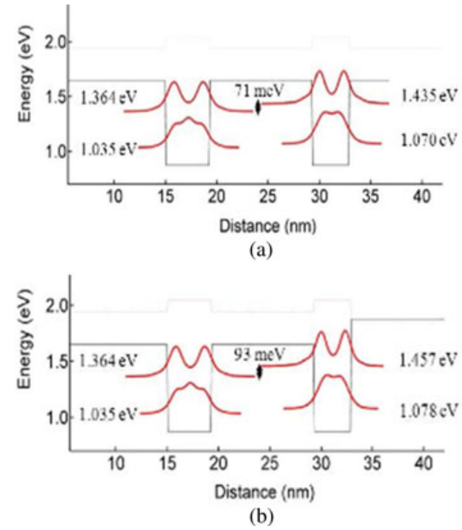

Fig. 6. Conduction band diagram and energy levels for a pair of uncoupled: (a) symmetric QWs and (b) asymmetric QWs, under no bias [12].

1) Uncoupled QWs Under No Bias: We take pairs of symmetric QWs and asymmetric QWs designed, such that, when coupled, the ground states are resonant at ~70 kV/cm field strength (see Fig. 6) [12] (the degree of symmetry is defined with respect to the outer barriers). The symmetric QW pair is composed of 4.3- and 3.6-nm-wide $In_{0.68}Ga_{0.32}As$ QWs separated by a 10 nm-thick $Al_{0.60}In_{0.40}As$ barrier and with $Al_{0.60}In_{0.40}As$ outer barriers. The asymmetric QW pair has the same structure except that the outer barrier on the right is taller: $Al_{0.75}In_{0.25}As$, than the outer barrier on the left. As can be seen, the energy separation between the excited states of the QW pairs $E_{1'1}$ is 93 and 71 meV for asymmetric QWs and symmetric QWs, respectively. The difference in $E_{1'1}$ values, $\Delta E_{1'1}$, stems from a well-known fact from quantum mechanics: increasing the barriers height(s) in a QW causes the excited states to increase faster in energy than the ground state [25]. This fact manifests itself in that the rightmost barrier of the asymmetric-QW pair "pulls up" the second-QW's first excited state much more than its ground state, with respect to the symmetric-QWs case (i.e., 22 meV versus 8 meV). That accounts for the 22 meV value for $\Delta E_{1'1}$.

2) Coupled QWs Under No Bias: The barrier between wells is reduced to 1.8 nm such that the QWs are coupled (see Fig. 7) [11], [26]. Due to spreading of the fields to adjacent wells, the $\Delta E_{1'1}$ value decreases from 22 to 18 meV. Now there are two

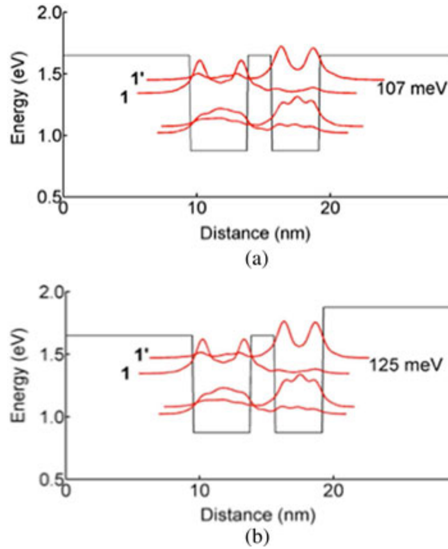

Fig. 7. Conduction band diagram and energy levels for a pair of coupled: (a) symmetric QWs and (b) asymmetric QWs, under no bias.

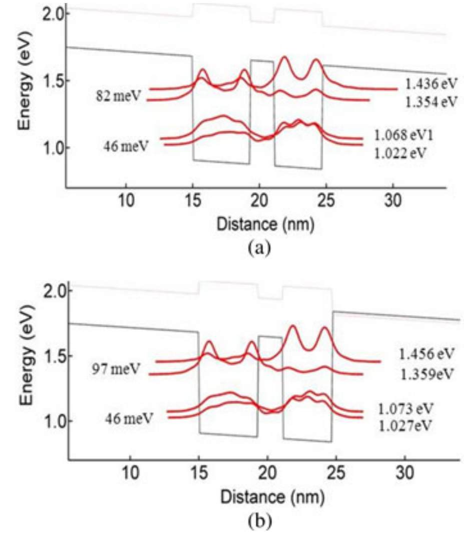

Fig. 8. Conduction band diagram and energy levels for a pair of coupled: (a) symmetric QWs and (b) asymmetric QWs, under a field of 70 kV/cm.

cases: symmetric coupled QWs (SCQW) and asymmetric coupled QWs (ACQW). For ACQW, the rightmost barrier "pushes" the symmetric excited state 1 to the left, while "pulling" the antisymmetric excited state $1'$ to the right. As a result, $z_{1'1'} - z_{11}$, the distance between the coordinates of the centroids of the electron-probability distributions for states $1'$ and 1 is larger for ACQW than for SCQW. It is well known [27], [28] that if $z_{1'1'} - z_{11}$ is nonzero, an applied electric field leads to changes in the energy-level separation, so-called first-order Stark effect. The effect has been used for electrically tuning the emission wavelength in interband cascade lasers [29] and QCLs [30]–[32] of diagonal transition. In all those laser-emission tuning cases, the field-induced energy differential δE increased with applied field. In our case, since the (excited) states are well below anticrossing, δE decreases with increasing applied field. That is, under an electric-field increment δF, the energy separation $E_{1'1}$ changes as such [26]

$$\delta E_{1'1} = -(z_{1'1'} - z_{11})\delta F q_0. \tag{8}$$

A similar behavior was reported by Sirtori *et al* [27] for states of coupled QWs that are below anticrossing (i.e., for states E_3 and E_2 in Fig. 3 of [27]). Since $z_{1'1'} - z_{11}$ is larger for ACQW than for SCQW, under the same applied electric field, the $E_{1'1}$ value will experience more Stark shift for ACQW than for SCQW structures. In turn, the $\Delta E_{1'1}$ value will *decrease* with increasing field.

3) Coupled QWs Under an Applied Field: We now apply a field of 70 kV/cm to the pairs of coupled QWs. As can be seen from Fig. 8, the $\Delta E_{1'1}$ value has decreased from 18 meV (i.e., the unbiased case in Fig. 7) to 15 meV, due to stronger Stark shift for ACQW than for SCQW. Thus, we can conclude that the net effect of tapering the barrier heights in asymmetric-coupled QWs, under an applied field, is to significantly increase the energy difference between their excited states compared to symmetric coupled QWs. Now, we can proceed to optimize TA-type structures for maximizing the $\Delta E_{1'1}$ value.

4) Linear Tapering: Taking the original unbiased ACQW structure [see Fig. 7(b)], we increase the height of both the central and rightmost barriers such that the barrier heights are linearly tapered (i.e., the central barrier becomes $Al_{0.80}In_{0.20}As$ and the rightmost barrier becomes AlAs) [26]. Now, the asymmetry has significantly increased [see top of Fig. 9(a)]. Then, we plot $\Delta E_{1'1}$ as a function of applied field for both cases [see Fig. 9(b)]. The increased asymmetry results in a much larger $\Delta E_{1'1}$ value under no bias (i.e., 40 meV versus 18 meV), but also in a stronger Stark effect, as expected, since $\Delta E_{1'1}$ decreases faster with applied field. Nonetheless, at 70 kV/cm, the $\Delta E_{1'1}$ value has virtually doubled (i.e., from 15 to 28 meV).

Applying linear tapering, we obtained the TA DW QCL design shown in Fig. 5. The E_{54} value has increased to 84 meV compared to 60 meV for DW QCLs. Furthermore, as discussed in the next section, the τ_{54} value is much larger than in conventional QCLs (i.e., 0.83 ps versus 0.25 ps). Both increases lead to a decrease in the RT $J_{\mathrm{leak,th}}/J_{\mathrm{th}}$ value from $\sim$15% in the case of conventional QCLs to $\sim$3% [12].

We would like to point out that the so-called shallow-well design [14], [33] is in effect a TA-type device, since a shallow barrier (adjacent to the shallow well), a normal-height barrier in the AR center and an exit barrier topped with an AlAs spike form a linear-taper TA-type structure, albeit without the benefit of deep QWs for cooling electrons in the upper laser level. The TA-type QCL reported by Bai *et al*. [14], [33], for an AR structure of single-phonon resonance (SPR) lower-level depopulation scheme, resulted in increasing the energy difference between the upper level and the next higher AR energy state E_{43} from 80 to $\sim$100 meV. While that suppressed leakage via state 4, hot electrons in state 3 cause hot electrons in the injector ground state that, in turn, significantly increase the backfilling current [12] which, together with the less efficient SPR depopulation scheme, may well explain why the $J_{\mathrm{th}}(300\ \mathrm{K})$ values are $\sim$30% higher than in conventional QCLs of same chip geometry [20].

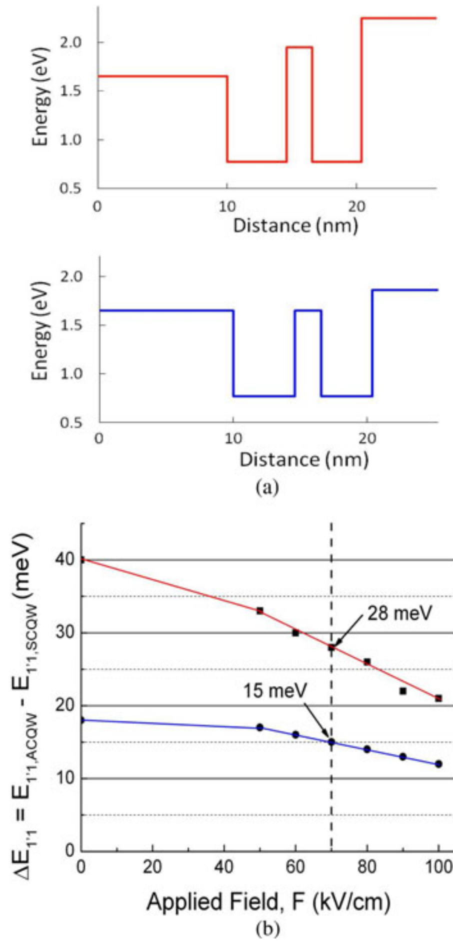

Fig. 9. (a) Band diagrams for ACQW (bottom) and linearly-tapered ACQW (top) and (b) $\Delta E_{1'1}$ as a function of applied field for each case.

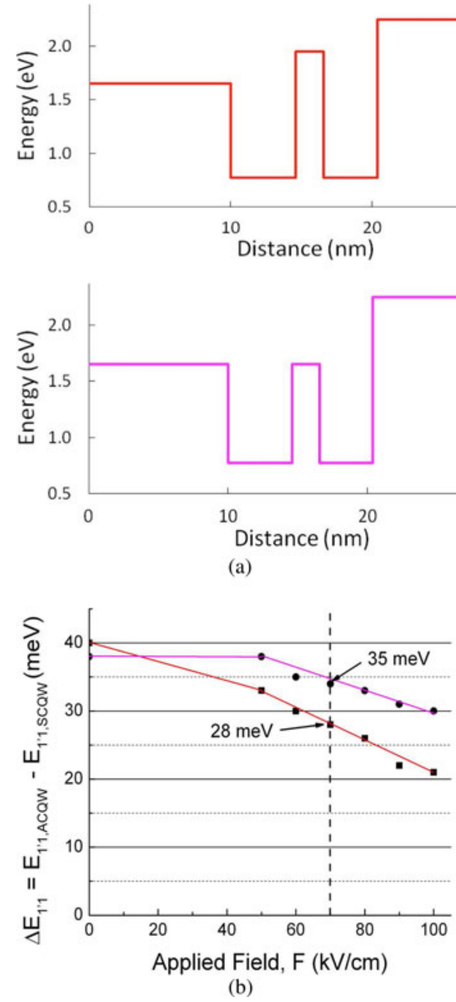

Fig. 10. (a) Band diagrams for linearly-tapered (top) and step-tapered (bottom) ACQW and (b) $\Delta E_{1'1}$ as a function of applied field for each case.

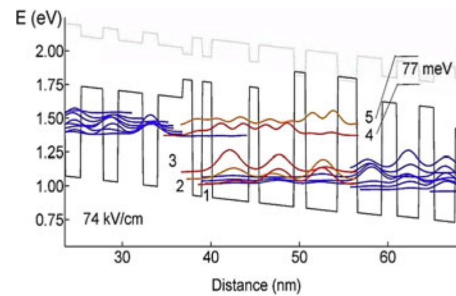

Fig. 11. Conduction band diagram and key wavefunctions for moderate-taper TA QCL structure emitting at $\lambda = 4.8$ μm [13]. The energy states 1 through 5 are defined just as in Fig. 1.

5) Step Tapering: We found earlier that strong asymmetry in linearly-tapered devices dramatically increases the $\Delta E_{1'1}$ value in the unbiased case, but, under applied field, the associated strong Stark shift undermines that effect to a moderate extent. Therefore, while keeping the tall rightmost barrier of the linear-taper TA design, we lower the central-barrier height to that of the leftmost barrier (i.e., to $Al_{0.60}In_{0.40}As$) [see bottom of Fig. 10(a)] in order to increase the coupling between QWs, thus, decreasing the $z_{1'1'} - z_{11}$ value and subsequently weakening the Stark effect. We name the TA-type structure thus obtained: step-taper TA (STA) QCL. As seen from the plot of $\Delta E_{1'1}$ versus applied field [Fig. 10(b)], while under no bias the $\Delta E_{1'1}$ values are basically the same for both cases, as the applied field increases, $\Delta E_{1'1}$ decreases much slower for the step-tapered case than for the linearly-tapered case. We take this as clear evidence that the Stark effect has been weakened. At 70 kV/cm the $\Delta E_{1'1}$ value is noticeably higher for step-tapered versus linearly-tapered devices (i.e., 35 meV versus 28 meV). This effect is more pronounced for structures with more than two QWs, such as the ARs of QCLs, as we will see in the next section.

B. Types of TA Deep-Well QCLs

Three types of TA DW QCLs are compared: 1) moderate taper [13] (see Fig. 11); 2) linear taper (see Fig. 5); and 3) step taper (see Fig. 12). There is increasing asymmetry by going from moderate-taper devices to step-taper devices. The asymmetry causes the antisymmetric states in the AR (colored in orange) to be "pulled" to the right. More specifically, for the excited AR states, state 5 is pulled to the right, which causes its

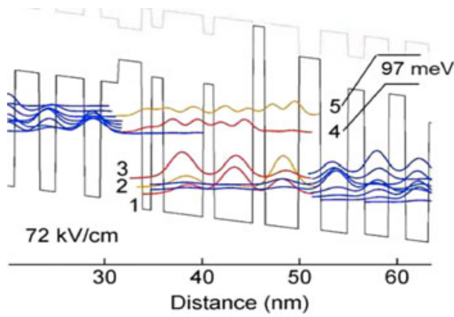

Fig. 12. Conduction band diagram and key wavefunctions for step-taper TA (STA) QCL structure emitting at λ = 4.7 μm. The energy states 1 through 5 are defined just as in Fig. 1.

TABLE II
COMPARISON OF LIFETIMES FOR VARIOUS QCLS

Lifetime	Moderate Taper	Linear Taper	Step Taper	Conventional
τ_{54}	0.75 ps	0.83 ps	1.17 ps	0.25 ps
τ_{42}	5.46 ps	6.10 ps	8.60 ps	4.33 ps
τ_{4}	1.51 ps	1.59 ps	1.68 ps	1.65 ps

wavefunction-overlap with state 4 to decrease and, in turn, the value of τ_{54} to increase. As shown in Table II, the τ_{54} value increases from 0.75 ps for moderate-taper devices to 1.17 ps for step-taper devices. That is, as seen for (3), the amount of carrier-leakage current steadily decreases with the increasing TA-structure asymmetry. Furthermore, due to reduced Stark shift, the step-taper device has the highest E_{54} value (i.e., 97 meV) that also substantially suppresses carrier leakage.

As for the ground states in the AR, state 2 is pulled to the right, which reduces its wavefunction-overlap with state 4, and thus causes the τ_{42} lifetime value to significantly increase (i.e., from 5.46 to 8.60 ps). In turn, the τ_4 value should also increase with increasing asymmetry. As seen from Table II, the τ_4 value indeed increases from 1.51 ps for moderately-tapered devices to 1.68 ps for step-tapered devices. Now, we see that by using the step-taper structure we have recovered τ_4 to a value close to that of conventional QCLs (i.e., 1.65 ps) while suppressing carrier leakage. That is, unlike in the case of DW devices, no price is paid in the J_{th}(300 K) value for achieving carrier-leakage suppression. We also note that step tapering has made state 2 to look very much like state 1 for conventional QCLs, that is, a lower AR state whose wavefunction has poor overlap with the upper-level wavefunction, thus ensuring a long upper-level lifetime.

The asymmetry also "pushes" the symmetric AR states to the left, but that hardly affects the τ_{41} and τ_{43} values since all relevant states move in the same direction. For instance, τ_{41} varies by only 10% when going from moderate-taper to step-taper cases (i.e., from 5.0 to 4.65 ps, and to 4.5 ps) while τ_{42} increases by 58% (see Table II). Since we have fabricated moderate-taper devices, next we compare them to conventional devices.

TABLE III
MODERATE TAPER VERSUS CONVENTIONAL QCL

Parameter	Moderate Taper QCL	Conventional QCL
τ_{4g}	1.30 ps	1.305 ps
τ_{3g}	0.22 ps	0.19 ps
$\tau_{\mathrm{up,g}}$	1.22 ps	1.23 ps
J_{leak} / J_{th} at 300K	~ 4.0 %	~15 %

C. Moderate-Taper TA Versus Conventional QCLs

The moderate-taper design is a stepwise approximation of the linear-taper design (see Fig. 5) for the purpose of easier fabrication. On the one hand, asymmetry causes the τ_4 value of moderate-taper devices to increase with respect to that of DW devices (i.e., 1.51 ps versus 1.32 ps) and thus approach the value for conventional devices. On the other hand, the tall barriers on the right side of the AR cause less penetration of the extractor states into the AR than in conventional QCLs. The two effects basically cancel each other out; the net effect being that the global values for state-4 and -3 lifetimes, and for the effective upper-level lifetime $\tau_{\mathrm{up},g}$ are pretty much the same for both cases (see Table III). That is, the first term in the J_{th} expression [see (1)] stays the same. However, carrier leakage is substantially suppressed since the E_{54} value increases to 77 meV and the τ_{54} value is three times larger than in conventional devices (see Table II). By using the same approach as in [4] for calculating the leakage-current density, but considering global values for both $\tau_{5,\mathrm{leak}}$ and $\tau_{5,\mathrm{tot}}$ lifetimes, we calculate a relative leakage-current density value $J_{\mathrm{leak}}/J_{\mathrm{th}}$ of $\sim$4%, that is, less than half that for DW devices and almost four times less than for conventional devices. Since $\tau_{\mathrm{up},g}$ is basically the same, an $\sim$11% decrease in J_{th}(300 K) value is expected, primarily due to carrier-leakage suppression.

D. Experimental Results From Moderate-Taper TA (Deep-Well) QCLs

Thirty-period QCL devices of active-region design shown in Fig. 11 were grown by MOCVD. Details of the growth, the material characterization, and the structure are provided in [13] and [34]. In Fig. 13(a), we show the light-current (*L–I*) curves in pulsed operation (100 ns, 2 kHz) for 3-mm-long, 19-μm-wide ridge, uncoated-facets devices as the heatsink temperature is varied. An inset shows that the devices lased at $\sim$4.8 μm. J_{th}(300 K) is 1.58 kA/cm^2, a value $\sim$14% less than for conventional QCLs of same geometry and similar injector-region doping level [4]. This agrees with the expected reduction in the J_{th}(300 K) value and is most likely a consequence of carrier-leakage suppression, as evidenced by high T_o and T_1 values [see Fig. 13(b)].

Fig. 13(b) shows, for two devices, the temperature dependence of both J_{th} and the slope efficiency over the 20–60 °C range in heatsink temperature. The T_o values are $\sim$230 K, typical of devices with suppressed carrier leakage and moderately high injector doping level [4], [14] as needed for

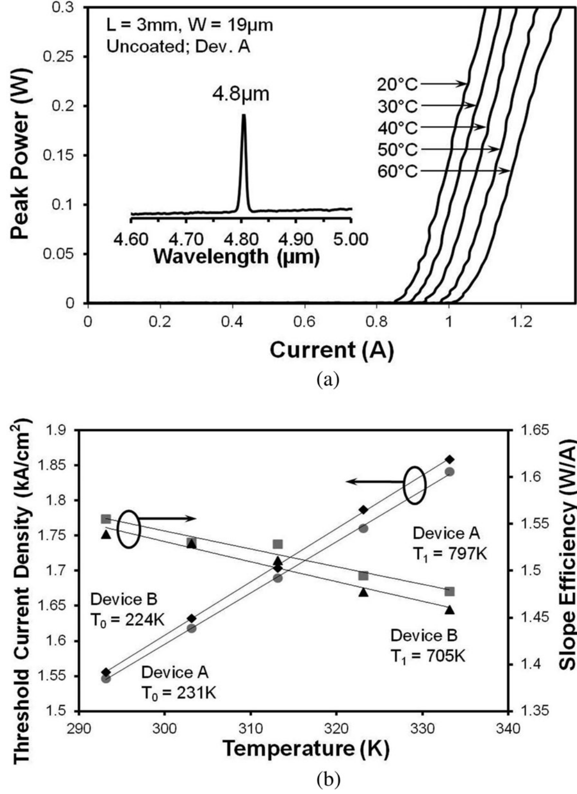

(a)

(b)

Fig. 13. (a) *L–I* curves in pulsed (100 ns, 2 kHz) mode at various heatsink temperatures, for device A. The threshold-current density $J_{\rm th}$ at 25 °C is 1.58 kA/cm^2. *Inset*: spectrum; (b) $J_{\rm th}$ and the slope efficiency as a function of heatsink temperature, for two devices. T_0 and T_1 are the characteristic temperature coefficients for $J_{\rm th}$ and the slope efficiency, respectively.

high-CW-power performance. A T_1 value of 797 K is measured which, to the best of our knowledge, is the highest T_1 value reported for mid-IR QCLs. On average, the T_1 values are ~750 K, that is, three times larger than the values for DW QCLs [4], [24] and more than twice the T_1 value (i.e., 348 K) for TA-QCLs without deep wells and of similar injector doping [14]. The latter is most likely due to much cooler electrons in the upper level of TA DW devices. That is, the energy differences between the upper level and the tops of the injection barrier and first barrier inside the AR are 420 and 400 meV, respectively, for this structure, while for the case of TA QCLs without deep wells [14], [33] those same energy differences are only 340 and 90 meV, respectively. Thus, for the latter case, there is rather poor coupling between the electrons in the upper level and the lattice, which, in turn, results in a high value for the electron-lattice coupling constant α [3], [35], thus leading to high electronic temperatures.

V. Step-Taper TA QCLs

A. Structure and Comparison to Conventional QCLs

The band diagram and relevant wavefunction moduli for the step-taper TA (STA)-QCL structure are shown in Fig. 12. The layer thicknesses (in Å) for one period, starting with the exit barrier, are ***22***, (28), [17], (25), [17], (24), *20*, 22, *22*, 20,

TABLE IV
Step Taper versus Conventional QCL

Parameter	Step-Taper QCL	Conventional QCL
τ_4	1.68 ps	1.65 ps
τ_{4g}	1.59 ps	1.305 ps
τ_{3g}	0.205 ps	0.19 ps
$\tau_{up,g}$	1.50 ps	1.23 ps
J_{leak} / J_{th} at 300K	~ 1.6 %	~ 15 %

23, 18, *25*, 17, *29*, 17, *18*, [24], **10**, [12], **41**, [11], **40**, ***<u>12</u>***, **35**. The bold normal scripts are $In_{0.68}Ga_{0.32}As$ QWs; bold italic script is an $Al_{0.75}In_{0.25}As$ barrier; bold italic, underlined script is an $Al_{0.85}In_{0.15}As$ barrier; bracketed normal scripts are $Al_{0.60}In_{0.40}As$ barriers; normal scripts are $In_{0.60}Ga_{0.40}As$ QWs; and italic scripts are $Al_{0.56}In_{0.44}As$ barriers. The layers in parentheses are part of the extractor region: one $In_{0.66}Ga_{0.34}As$ QW and two $In_{0.64}Ga_{0.36}As$ QWs. By comparison to the moderate-taper TA device structure (see Fig. 11), the first two barriers have been lowered (i.e., from $Al_{0.65}In_{0.35}As$ to $Al_{0.60}In_{0.40}As$) while the third barrier has been raised (i.e., from $Al_{0.75}In_{0.25}As$ to $Al_{0.85}In_{0.15}As$). Thus, the asymmetry of the structure has been significantly increased and one has true step tapering [i.e., two relatively shallow barriers followed by a relatively tall barrier, just like at the bottom of Fig. 10(a)]. The splitting at resonance between the injector ground state g and the upper level is 5 meV at a field of 78 kV/cm. All calculations are done for a field of 72 kV/cm, for which the energy difference between the upper level and state g is 9 meV.

A comparison between the STA and conventional QCL structures is shown in Table IV. As discussed earlier, the τ_4 values are similar since the asymmetry of the STA device causes τ_{42} to have a similar large value as τ_{41} for conventional devices (i.e., 8.60 ps versus 9.08 ps). However, due to tall barriers on the right side of the AR, penetration of states from the extractor into the AR is much less than in conventional QCLs, thus, resulting in higher global upper-state and global effective upper-state lifetimes. In particular, $\tau_{{\rm up},g}$ is 22% higher for STA QCLs than for conventional QCLs (i.e., 1.50 ps versus 1.23 ps). Thus, in addition to carrier-leakage suppression, one can also achieve significantly increased upper-level lifetime. As for carrier leakage, it is virtually suppressed because of two factors: a large E_{54} value (97 meV) and a τ_{54} value almost five times larger than for conventional devices (see Table II). Using the same procedure as for moderate-taper devices, we find the relative leakage-current density $J_{\rm leak,th}/J_{\rm th}$ value to be ~1.6%, that is, almost an order of magnitude less than that for conventional QCLs and for all practical purposes negligible. Then, the $J_{\rm th}$(300 K) value is estimated to decrease by at least 25% compared to that for conventional devices, due both to carrier-leakage suppression and higher global upper-state lifetime. A 25% decrease in $J_{\rm th}$(300 K) may appear modest, but when coupled with higher T_0 values for TA-type devices (i.e., ~240 K versus ~140 K for conventional devices) it makes a significant difference, as seen from Fig. 14. Basically, the $J_{\rm th}$ value for STA QCLs at a heatsink temperature of 370 K is the same as the $J_{\rm th}$ value for conventional QCLs at 300 K. This should lead

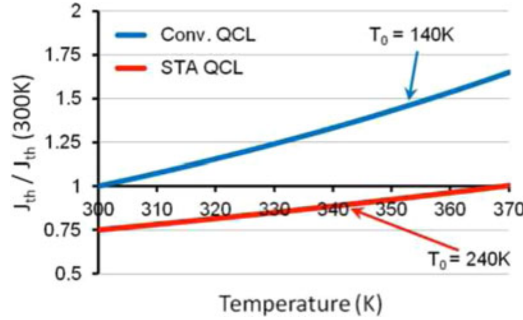

Fig. 14. Schematic comparison between the values of the ratio of threshold-current density J_{th} to RT conventional-QCL J_{th} for STA QCLs and conventional QCLs, when taking typical T_0 values for each case. The J_{th} value of STA QCLs at 370 K heatsink temperature is approximately the 300 K J_{th} value for conventional QCLs.

to much less heating and to higher CW operating temperatures than for conventional mid-IR QCLs.

B. Extension of the Concept to Shorter Wavelengths ($\lambda = 3.5$–4.0 μm)

While the aforementioned discussions have focused on QCLs emitting in the 4.5–5.0-μm wavelength range, the STA concept is also applicable to shorter emission-wavelength λ QCLs. As λ decreases below 4 μm, achieving strong electron confinement to the QCL active regions becomes increasingly difficult, because of the larger transition energies. To accommodate those, deeper wells and taller barriers (i.e., higher strain layers) are necessary to avoid excessive carrier leakage. However, the use of high-strain (>1.5%) layers, throughout the core region, has been found [36]–[38] to result in significantly lower G_{th} values than in conventional mid-IR, InP-based QCLs. More specifically, Lee and Yu [36] find the G_{th} value of 3.8-μm QCLs, containing layers of 1.6% strain, to be ~30% smaller than those of 4.3-μm QCLs, containing layers of 1% strain, and ascribe the difference to a 30% decrease in cross-plane thermal conductivity as a consequence of poor-quality interfaces. Their results are corroborated by an ~27% lower G_{th} value obtained for 3.76-μm QCLs, with 1.6% and 1.8% strained layers [37], by comparison to conventional mid-IR QCLs (i.e., ≤1% strain). Shorter-wavelength (λ ~3.56 μm) QCLs [38] of core regions composed of alternating strained layers: 1.9% and 2.3% strain, respectively, while exhibiting moderately low electron leakage (e.g., pulsed T_1 values of ~190 K), have G_{th} values ~40% smaller than those of 4.5–5.0-μm QCLs of same geometry and mounting configuration; in turn, leading to highly temperature sensitive device characteristics (e.g., T_1, in CW operation, reaches values as low as 38 K) [38]. As the critical thicknesses for strain relaxation are approached, it is anticipated that device reliability may deteriorate through thermally activated relaxation processes. As an alternate approach to mitigate this strain-relaxation issue as well as to lower the layers' strain to values typical of 4.5–5.0-μm-emitting QCLs, metamorphic buffer layers (MBLs) can be utilized as virtual substrates of a specified lattice constant, thus opening up the palette of III/V alloys available for new device architectures [39], [40]. A 3.6-μm-emitting STA structure design has been reported, based on a virtual substrate of 0.577-nm lattice constant that corresponds to relaxed $In_{0.30}Ga_{0.70}As$ (representing the top part of the MBL) [39]. The design benefits are large barrier heights in the AR and a large E_{54} value (85 meV), thereby ensuring a low electron temperature in the upper level as well as carrier-leakage suppression. Furthermore, the strain-thickness products for layers employed in the AR are comparable to those employed in longer wavelength (4.8 μm emitting) TA QCLs grown directly on InP substrates [34].

C. Projection of Maximum Wallplug Efficiency in Pulsed and CW Operation

First, we estimate the maximum, RT pulsed wallplug-efficiency $\eta_{\mathrm{wp,max}}$ value by using (5). Since the STA-QCL device virtually suppresses carrier leakage, we take values of 3.0 and 0.9 for parameters B and η_s, respectively, as derived from published data on TA-like devices with suppressed carrier leakage [14]. Similarly, for $\alpha_{m,\mathrm{opt}}$, we take a value of 2.2 cm^{-1} that was found to maximize the pulsed wallplug efficiency in two experimental reports [14], [20] employing 40-period core regions. Then, for a 40-period STA device, the projected single-facet, RT $\eta_{\mathrm{wp,max}}$ pulsed value is ≈29%, a value quite close to theoretically predicted values [15], [16] for QCLs of 4.8-μm emission wavelength (≈31%).

For the CW $\eta_{\mathrm{wp,max}}$ projection, we consider a 40-period, 5-mm-long STA-QCL device of similar thermal and electrical resistances as for conventional QCLs of 8-μm-wide buried ridge, and the experimentally obtained T_o and T_1 values from moderate-taper TA QCLs [13]. Note that within one period of the STA structure there are only four interfaces involving two highly strained materials [i.e., the $Al_{0.85}In_{0.15}As$ (2.5% strain) and $Al_{0.75}In_{0.25}As$ (1.8% strain) barriers] out of a total of 50 interfaces. Thus, the effect of those high-strain layers on the R_{th} value should be minimal, and that is why we believe our assumption of similar R_{th} value for STA devices compared to conventional devices is justified. Then, by using (6) and (7) with an R_{th} value of 1.7 K/W, $\Delta T_{\mathrm{act}}|_{\eta_{\mathrm{wp,max}}}$ is found be ≈16 K. In contrast, for conventional QCLs [9], the calculated $\Delta T_{\mathrm{act}}|_{\eta_{\mathrm{wp,max}}}$ value, for an 8-μm-wide buried ridge, is ≈30 K, that is, almost twice that estimated for STA QCLs. Furthermore, for the TA QCL without deep wells [14], the calculated $\Delta T_{\mathrm{act}}|_{\eta_{\mathrm{wp,max}}}$ value is ≈49 K since the estimated R_{th} value is found to be ~1.8 times the R_{th} value of conventional QCLs of same geometry (i.e., 3.1 K/W versus 1.7 K/W). The significantly higher R_{th} value may well be due to the 14 interfaces, per period, involving heavily strained (3.5%) AlAs layers, corresponding to tall portions of the exit barrier and all barrier layers in the extractor and the injector, thus explaining why the pulsed $\eta_{\mathrm{wp,max}}$ value is ~30% higher than the CW one (i.e., 27% versus 21%). Notwithstanding, the CW $\eta_{\mathrm{wp,max}}$ value is a record value for QCLs, due to the high T_o and T_1 values caused by the TA-type AR structure. Finally, for the STA QCL the projected single-facet, RT $\eta_{\mathrm{wp,max}}$ CW value is ≈27%. That is, a value only 7% smaller than the pulsed value, thus close to

theoretically predicted limits for 4.8 μm-emitting devices. The use of the pocket-injector design [23] for STA-type ARs with deep wells may well increase the RT $\eta_{\mathrm{wp,max}}$ CW value beyond 30%.

VI. Conclusion

Carrier leakage in mid-IR QCLs is due to relatively small energy differentials between the upper laser level and the next higher AR energy state E_{54}, and the existence of hot electrons in the upper level. To suppress it one needs to increase the E_{54} value and reduce the overlap of the upper-level and next-higher AR-state wavefunctions (i.e., maximize the τ_{54} value), while making sure that carriers in the upper level remain relatively cool (e.g., via the use of deep-well ARs).

By designing QCL structures with QWs and barrier layers of varying compositions (i.e., multidimensional conduction-band engineering) one can both maximize the E_{54} and τ_{54} values as well as minimize the electronic temperature in the upper level. TA QCLs have resulted in significant suppression of the carrier leakage as evidenced by record-high T_1 values (797 K) from devices with deep wells, and record-high CW wallplug efficiency (21%) from devices without deep wells.

Strong asymmetry as well as Stark-shift reduction in STA deep-well QCLs leads to more than doubling the E_{54} value and almost a fivefold increase in the τ_{54} value compared to conventional QCLs which, in turn, results in virtually complete carrier-leakage suppression (i.e., $J_{\mathrm{leak}}/J_{\mathrm{th}} \approx 1.6\%$). In addition, for STA QCL devices the global upper-level lifetime can be increased by at least 20%. The combined effect of carrier-leakage suppression and upper-level lifetime increase leads to an overall decrease in the RT J_{th} value of at least 25%. In turn, the projected pulsed and CW RT wallplug-efficiency values are $\approx$29% and $\approx$27%, that is, close to maximum theoretically predicted values for QCLs emitting in the 4.5–5.0-μm wavelength range. Then, the dissipated heat decreases by a factor of $\sim$2.5 compared to conventional QCLs, which is important since thermal-load management drives the packaged laser weight. Furthermore, since the core-region temperature rise at the maximum CW wallplug-efficiency point becomes comparable to the core-region temperature rise at threshold in conventional QCLs (i.e., $\sim$15 K) [9] and QCL-device degradation has been directly related to device heating [41] long-term reliable operation would become possible at high (>0.5 W) CW powers.

Multidimensional conduction-band engineering for optimizing the CW performance of mid-IR QCLs can be realized by any advanced crystal-growth technique since it has already been demonstrated by using both MOCVD or gas-source MBE, and can be implemented with MBE by using multiple effusion cells as sources of elements such as In, Ga, and Al.

Note Added in Proof: We have just become aware that Semtsiv *et al.*, by using gas-source MBE, have achieved 3.9 μm-emitting TA-type QCLs of low thresholds, due primarily to less influence of the interface scattering on the upper-level lifetime [43] and that, in the process, carrier leakage was, as expected, substantially suppressed: T_1 values of 550 K [44]. While we have not taken into account interface scattering, it is now apparent that by applying Semtsiv *et al.*'s ingenious analysis, STA QCLs are likely to provide even lower than projected J_{th} (300 K) values by comparison to conventional QCLs, since the upper-level wavefunction "sees" only $\sim$six interfaces by comparison to $\sim$eight interfaces for conventional QCLs, and the lower level should depopulate faster than in conventional QCLs.

Acknowledgment

The authors are grateful to J. Faist and S. Kumar for valuable technical discussions.

References

[1] J. Faist, F. Capasso, C. Sirtori, D. Sivco, and A. Cho, "Intersubband transitions in quantum wells: Physics and device applications II," in *Semiconductors and Semimetals*, vol. 66, H. Liu and F. Capasso, Eds. New York: Academic, 2000, ch. 1, pp. 1–83.

[2] D. Botez, J. C. Shin, S. Kumar, L. J. Mawst, I. Vurgaftman, and J. R. Meyer, "Electron leakage and its suppression via deep-well structures in 4.5–5.0 μm-emitting quantum cascade lasers," *Opt. Eng.*, vol. 49, pp. 111108-1–111108-9, 2010.

[3] M. S. Vitiello, T. Gresch, A. Lops, V. Spagnolo, G. Scamarcio, N. Hoyler, M. Giovannini, and J. Faist, "Influence of InAs, AlAs δ layers on the optical, electronic, and thermal characteristics of strain-compensated GaInAs/AlInAs quantum-cascade lasers," *Appl. Phys. Lett.*, vol. 91, pp. 161111-1–161111-3, 2007.

[4] D. Botez, S. Kumar, J. C. Shin, L. J. Mawst, I. Vurgaftman, and J. R. Meyer, "Temperature dependence of the key electro-optical characteristics for midinfrared emitting quantum cascade lasers," *Appl. Phys. Lett.*, vol. 97, pp. 071101-1–071101-3, 2010.

[5] A. Bismuto, R. Terazzi, M. Beck, and J. Faist, "Influence of the growth temperature on the performances of strain balanced quantum cascade lasers," *Appl. Phys. Lett.*, vol. 98, pp. 091105-1–091105-3, 2011.

[6] M. Razeghi, "High-power high-wallplug efficiency mid-infrared quantum cascade lasers based on the InP/ GaInAs/AlInAs material system," *Proc. SPIE*, vol. 7230, pp. 723011-1–723011-8, 2009.

[7] F. Xie, C. Caneau, H. P. LeBlanc, N. J. Visovsky, S. C. Chaparala, O. D. Deichmann, L. C. Hughes, C. Zah, D. P. Caffey, and T. Day, "Room temperature CW operation of short wavelength quantum cascade lasers made of strain balanced $\mathrm{Ga}_x\mathrm{In}_{1-x}\mathrm{As}/\mathrm{Al}_y\mathrm{In}_{1-y}\mathrm{As}$ material on InP substrates," *IEEE J. Sel. Top. Quantum Electron.*, vol. 17, no. 5, pp. 1445–1452, Sep./Oct. 2011.

[8] Y. Bai, S. Slivken, S. R. Darvish, and M. Razeghi, "Room temperature continuous wave operation of quantum cascade lasers with 12.5% wall plug efficiency," *Appl. Phys. Lett.*, vol. 93, pp. 021103-1–021103-3, 2008.

[9] A. Lyakh, R. Maulini, A. Tsekoun, R. Go, C. Pflügl, L. Diehl, Q. J. Wang, F. Capasso, C. Kumar, and N. Patel, "3 W continuous-wave room temperature single-facet emission from quantum cascade lasers based on nonresonant extraction design approach," *Appl. Phys. Lett.*, vol. 95, pp. 141113-1–141113-1, 2009.

[10] J. C. Shin, M. D'Souza, Z. Liu, J. Kirch, L. J. Mawst, D. Botez, I. Vurgaftman, and J. R. Meyer, "Highly temperature insensitive, deep-well 4.8 μm emitting quantum cascade semiconductor lasers," *Appl. Phys. Lett.*, vol. 94, pp. 201103-1–201103-3, 2009.

[11] J. Shin, "Tapered Active-region quantum cascade laser," in Very low temperature sensitive, deep-well quantum cascade lasers (λ = 4.8 μm) grown by MOCVD, PhD thesis, ch. 6, pp. 92–103, University of Wisconsin-Madison, Aug. 2010. [Online]. Available: http://digital.library.wisc.edu/1793/52493

[12] D. Botez, J. C. Shin, S. Kumar, J. Kirch, C.-C. Chang, L. J. Mawst, I. Vurgaftman, J. R. Meyer, A. Bismuto, B. Hinkov, and J. Faist, "The temperature dependence of key electro-optical characteristics for mid-infrared emitting quantum cascade lasers," *Proc. SPIE Novel In-Plane Semicond. Lasers X Conf.*, vol. 7953, pp. 79530N-1–79530N-12, Feb. 2011.

[13] J. D. Kirch, J. C. Shin, C.-C. Chang, L. J. Mawst, D. Botez, and T. Earles, "Tapered active-region quantum cascade lasers (λ = 4.8 μm) for virtual suppression of carrier-leakage currents," *Electron. Lett.*, vol. 48, pp. 234–235, Feb. 2012.

[14] Y. Bai, N. Bandyopadhyay, S. Tsao, S. Slivken, and M. Razeghi, "Room temperature quantum cascade lasers with 27% wall plug efficiency," *Appl. Phys. Lett.*, vol. 98, pp. 181102-1–181102-3, 2011.
[15] J. Faist, "Wallplug efficiency of quantum cascade lasers: Critical parameters and fundamental limits," *Appl. Phys. Lett.*, vol. 90, pp. 253512-1–253512-3, 2007.
[16] Q. K. Yang, C. Schilling, R. Ostendorf, S. Hugger, F. Fuchs, and J. Wagner, "Wall-plug efficiency of mid-infrared quantum cascade lasers," *J. Appl. Phys.*, vol. 111, pp. 053111-1–053111-9, 2012.
[17] D. Botez, "Comment on "Highly temperature insensitive quantum cascade lasers" [Appl. Phys. Lett. 97, 251104, (2010)]," *Appl. Phys. Lett.*, vol. 98, p. 216101, May 2011.
[18] P. M. Smowton and P. Blood, "The differential efficiency of quantum well lasers," *IEEE J. Sel. Top. Quantum Electron.*, vol. 3, no. 2, pp. 491–498, Apr. 1997.
[19] D. Botez, "Design considerations and analytical approximations for high continuous-wave power, broad-waveguide diode lasers," *Appl. Phys. Lett.*, vol. 74, pp. 3102–3104, May 1999.
[20] R. Maulini, A. Lyakh, A. Tsekoun, R. Go, C. Pflügl, L. Diehl, F. Capasso, C. Kumar, and N. Patel, "High power thermoelectrically cooled and uncooled quantum cascade lasers with optimized reflectivity facet coatings," *Appl. Phys. Lett.*, vol. 95, pp. 151112-1–151112-3, 2009.
[21] A. Evans, S. R. Darvish, S. Slivken, J. Nguyen, Y. Bai, and M. Razeghi, "Buried heterostructure quantum cascade lasers with high continuous-wave wall plug efficiency," *Appl. Phys. Lett.*, vol. 91, pp. 071101-1–071101-3, 2007.
[22] Y. Bai, S. R. Darvish, S. Slivken, W. Zhang, A. Evans, J. Nguyen, and M. Razeghi, "Room temperature continuous wave operation of quantum cascade lasers with watt-level optical power," *Appl. Phys. Lett.*, vol. 92, pp. 101105-1–101105-3, 2008.
[23] A. Bismuto, R. Terazzi, B. Hinkov, M. Beck, and J. Faist, "Fully automatized quantum cascade laser design by genetic optimization," *Appl. Phys. Lett.*, vol. 101, pp. 021103-1–021103-3, 2012.
[24] J. C. Shin, L. J. Mawst, D. Botez, I. Vurgaftman, and J. R. Meyer, "Ultra-low temperature sensitive, deep-well quantum-cascade lasers ($\lambda = 4.8\ \mu$m) via uptapering the conduction band edge of injector regions," *Electron. Lett.*, vol. 45, pp. 741–742, 2009.
[25] J. P. McKelvey, *Solid State and Semiconductor Physics*. New York: Harper & Row, 1966, ch. 4, pp. 88–91.
[26] D. Botez, J. C. Shin, J. D. Kirch, C.-C. Chang, L. J. Mawst, and T. Earles, "Tapered active-region, mid-infrared quantum cascade lasers for complete suppression of carrier-leakage currents," *Proc. SPIE Novel In-Plane Semicond. Lasers XI Conf.*, vol. 8277, pp. 82770W-1–82770W-9, Feb. 2012.
[27] C. Sirtori, F. Capasso, D. L. Sivco, A. L. Hutchinson, and A. Y. Cho, "Resonant Stark tuning of second-order susceptibility in coupled quantum wells," *Appl. Phys. Lett.*, vol. 60, pp. 151–153, 1992.
[28] J. Faist, F. Capasso, C. Sirtori, D. L. Sivco, A. L. Hutchinson, and A. Y. Cho, "Laser action by tuning the oscillator strength," *Nature (London)*, vol. 387, pp. 777–782, 1997.
[29] S. Suchalkin, M. V. Kisin, S. Luryi, G. Belenky, F. J. Towner, J. D. Bruno, C. Monroy, and R. L. Tober, "Widely tunable type-II interband cascade laser," *Appl. Phys. Lett.*, vol. 88, pp. 031103-1–031103-3, 2006.
[30] Y. Yao, Z. Liu, A. J. Hoffman, K. J. Franz, and C. F. Gmachl, "Voltage tunability of quantum cascade lasers," *IEEE J. Quantum Electron.*, vol. 45, no. 6, pp. 730–736, Jun. 2009.
[31] Y. Yao, K. J. Franz, X. Wang, J.-Y. Fan, and C. Gmachl, "A widely voltage-tunable quantum cascade laser based on "two-step" coupling," *Appl. Phys. Lett.*, vol. 95, pp. 021105-1–021105-3, 2009.
[32] A. Bismuto, R. Terazzi, M. Beck, and J. Faist, "Electrically tunable, high performance quantum cascade laser," *Appl. Phys. Lett.*, vol. 96, pp. 141105-1–141105-3, 2010.
[33] Y. Bai, N. Bandyopadhyay, S. Tsao, E. Selcuk, S. Slivken, and M. Razeghi, "Highly temperature insensitive quantum cascade lasers," *Appl. Phys. Lett.*, vol. 97, pp. 251104-1–251104-3, 2010.
[34] J. C. Shin, L. J. Mawst, and D. Botez, "Crystal growth via metal-organic vapor phase epitaxy of quantum-cascade-laser structures composed of multiple alloy compositions," *J. Cryst. Growth*, vol. 357, pp. 15–19, 2012.
[35] V. Spagnolo, G. Scamarcio, W. Schrenk, and G. Strasser, "Influence of the band-offset on the electronic temperature of GaAs/Al(Ga)As superlattice quantum cascade lasers," *Semicond. Sci. Technol.*, vol. 19, pp. S110–S112, 2004.
[36] H. K. Lee and J. S. Yu, "Thermal analysis of short wavelength InGaAs/InAlAs quantum cascade lasers," *Solid-State Electron.*, vol. 54, pp. 769–776, 2010.
[37] N. Bandyopadhyay, Y. Bai, B. Gokden, A. Myzaferi, S. Tsao, S. Slivken, and M. Razeghi, "Watt level performance of quantum cascade lasers in room temperature continuous wave operation at $\lambda \sim 3.76\ \mu$m," *Appl. Phys. Lett.*, vol. 97, pp. 131117-1–131117-3, 2010.
[38] N. Bandyopadhyay, S. Slivken, Y. Bai, and M. Razeghi, "High power, continuous wave, room temperature operation of $\lambda \sim 3.4\ \mu$m and $\lambda \sim 3.55\ \mu$m InP-based quantum cascade lasers," *Appl. Phys. Lett.*, vol. 100, pp. 212104-1–212104-3, 2012.
[39] L. J. Mawst, J. D. Kirch, C.-C. Chang, T. Kim, T. Garrod, D. Botez, S. Ruder, T. F. Kuech, T. Earles, R. Tatavarti, N. Pan, and A. Wibowo, "InGaAs/AlInAs strain-compensated superlattices grown on metamorphic buffer layers for low-strain, 3.6 μm-emitting quantum-cascade-laser active regions," *J. Cryst. Growth*, to be published. [Online]. Available: http://dx.doi.org/10.1016/j.jcrysgro.2012.06.053
[40] K. L. Schulte, T. J. Garrod, T. W. Kim, J. Kirch, S. Ruder, L. J. Mawst, and T. F. Kuech, "Metalorganic vapor phase growth of quantum well structures on thick metamorphic buffer layers grown by hydride vapor phase epitaxy," *J. Cryst. Growth*, to be published. [Online]. Available: http://dx.doi.org/10.1016/j.jcrysgro.2012.08.053
[41] Workshop on challenges in power scaling of semiconductor diode laser emitters and arrays: Heat management, reliability, and beam control, U.S. Army Research Office, Contract No. W911NF-11-1-0463, Final Report, Jun. 2012.
[42] D. Botez and J. C. Shin, "High power, high efficiency quantum cascade lasers with reduced electron leakage," U.S. Patent, US 8,325,774 B2, Dec. 2012.
[43] M. P. Semtsiv, Y. Flores, M. Chashnikova, G. Monastyrskyi, and W. T. Masselink, "Low-threshold intersubband laser based on interface-scattering-rate engineering," *Appl. Phys. Lett.,* vol. 100, pp. 163502-1–163502-3, 2012.
[44] Y. V. Flores, M. P. Semtsiv, M. Elagin, G. Monastyrskyi, S. Kurlov, A. Aleksandrova, J. Kischkat, and W. T. Masselink, "Thermally activated leakage current in high-performance short-wavelength quantum cascade lasers," *J. Appl. Phys.*, vol. 113, pp. 134506-1–134506-10, 2013.

Dan Botez (S'71–M'79–SM'85–F'86) was born in Bucharest, Romania, in May 1948. He received the B.S. degree (with Highest Honors) and the M.S. and Ph.D. degrees in electrical engineering from the University of California, Berkeley, in 1971, 1972, and 1976, respectively.

In 1977, he joined RCA Laboratories, Princeton, NJ, where his research concentrated on new types of high-power, single-mode AlGaAs/GaAs lasers, which became commercial products. In 1986, he joined TRW Inc., Redondo Beach, CA, where he was a Senior Staff Scientist and a Technical Fellow. At TRW, he co-invented the concept of resonantly (leaky-wave) coupled phase-locked laser array of antiguides (1988) which constituted to the first Photonic-Crystal (PC) laser for single-spatial-mode operation from wide-aperture ($\geq 100\ \mu$m) devices. As a result, in 1990, he led the team that "broke" the 1-W coherent-power barrier for diode lasers. Since 1993, he has been the Philip Dunham Reed Professor of electrical engineering at the University of Wisconsin-Madison (UW-Madison), Madison. At UW-Madison his initial research resulted in record high CW power and wallplug efficiency from near-infrared diode lasers. Work on grating surface-emitting lasers led in 2000 to the concept of using a π phase shift in the grating center for single-lobe surface emission at no penalty in efficiency. Recent work has focused in two key research areas for mid-infrared, quantum cascade lasers: complete carrier-leakage suppression and PC-type devices for realizing single-spatial-mode operation to watt-range CW powers. He has authored or coauthored more than 390 technical publications (h-index: 37) of which 300 were refereed, and holds 51 patents.

Prof. Botez is a member of Phi Beta Kappa and a Fellow of the Optical Society of America (OSA). In 1979, he received an RCA Outstanding Achievement Award for co-development of high-density optical recording using diode lasers. As part of the IEEE centennial (1984) events, he was chosen the Outstanding Young Engineer of the IEEE Photonics Society. In 1984, he co-initiated the IEEE Photonics Society Semiconductor Laser Workshop, which is now held annually. In 1995, he was awarded the "Doctor Honoris Causa" degree by the Polytechnical University of Bucharest, and in 2010, he was the recipient the OSA Nick Holonyak Jr. Award.

Jae Cheol Shin was born in Korea in 1975. He received the B.S. and M.S. degrees in physics from Kyung Hee University, Yongin, Korea, in 2001 and 2003, respectively, and the Ph.D. degree in electrical engineering from the University of Wisconsin-Madison, Madison, in 2010.

At the University of Wisconsin-Madison his research focused on highly temperature insensitive, deep-well quantum cascade lasers, as well as III-V semiconductor growth using metal organic chemical vapor deposition (MOCVD). After graduation, he was with the Department of Electrical and Computer Engineering, University of Illinois at Urbana-Champaign as a Postdoctoral Fellow pursuing research in InGaAs nanowire growth using MOCVD for various electronic- and photonic-device applications. He is currently a Senior Researcher in photonics-energy center at the Korea Photonics Technology Institute, Gwangju, Korea, where he has researched novel III-V compound semiconductor devices. He has authored or coauthored more than 30 technical papers.

Jeremy Daniel Kirch (M'12) was born in Madison, Wisconsin, in 1983. He received the B.S. degree in both electrical engineering and physics from the University of Wisconsin–Madison, Madison, in 2007, where he is currently working toward the Ph.D. degree in the Department of Electrical and Computer Engineering, as a Roger Bacon Fellowship recipient.

His graduate studies have primarily consisted of investigations into compressively strained metamorphic buffer layers grown by MOCVD on either InP or GaAs, including InAsP, InPSb, and InGaAs MBLs, for use with Type-I QW Lasers. More recently, his research efforts have been focused on quantum cascade laser (QCL) design, fabrication, and testing, including research into high-power QCL phase-locked arrays.

Chun-Chieh Chang was born in Taiwan. He is currently working toward the Ph.D. degree in the Department of Electrical and Computer Engineering, University of Wisconsin-Madison, Madison.

His research interests include physics of semiconductor nanostructures, semiconductor quantum-confinement devices, nanofabrication, novel material processing and characterization, low-temperature and high magnetic field measurement, plasmonics, and nanophotonics.

Luke J. Mawst (M'88–SM'93–F'11) received the B.S. degree in engineering physics and the M.S. and Ph.D. degrees in electrical engineering all from the University of Illinois at Urbana-Champaign, Champaign, in 1982, 1984, and 1987, respectively. His dissertation research involved the development of index-guided semiconductor lasers and laser arrays grown by metal-organic chemical vapor deposition (MOCVD).

He joined TRW Inc., Redondo Beach, CA, in 1987, where he was a Senior Scientist in the TRW Research Center, engaged in the design and development of semiconductor lasers using MOCVD crystal growth. He is a Co-Inventor of the resonant optical waveguide (ROW) antiguided-array concept and has contributed to its development as a practical source of high coherent power. He developed a novel, single-mode edge-emitting laser structure; the ARROW laser, as a source for coupling high powers into single-mode optical fibers. He is currently a Professor in the Department of Electrical and Computer Engineering, University of Wisconsin–Madison, Madison, where he is involved in the development of novel III–V compound semiconductor device structures, including vertical-cavity surface emitters, active-photonic-crystal structures, dilute-nitride lasers, solar cells, lasers employing metamorphic buffer layers, and quantum cascade lasers. He is a Founder of Alfalight Inc., a Madison-based manufacturer of high-power diode lasers. He is the author or coauthor of more than 200 technical papers and holds 22 patents.

Dr. Mawst received the TRW Group Level Chairman's Award for his contribution in the development of ROW antiguided-array concept.

Thomas Earles received the B.S. degree from Northeastern University, Boston, MA, in 1993, and the M.S. degree from the University of Wisconsin–Madison, Madison, in 1996.

In 1999, he co-founded Alfalight, Inc., after leaving the doctoral program at the University of Wisconsin, and actively participated in its management. At Alfalight, a high-power diode-laser manufacturing company, he led the development of the highest power, telecom-qualified, 980-nm pump lasers commercially available at the time. He is currently the Director of Product Development at Intraband, LLC, Madison, WI, where his research includes the development and commercialization of high-power quantum cascade lasers. He actively collaborates with researchers at the University of Wisconsin-Madison and is an Honorary Fellow in the Department of Electrical and Computer Engineering.